NANO LETTERS

pubs.acs.org/NanoLett Letter

Topology Classification using Chiral Symmetry and Spin Correlations in Graphene Nanoribbons

Jingwei Jiang and Steven G. Louie*

Cite This: *Nano Lett.* 2021, 21, 197−202 Read Online

ACCESS | Metrics & More | Article Recommendations | Supporting Information

ABSTRACT: We apply the topological classification theory using chiral symmetry to graphene nanoribbons (GNRs). This approach eliminates the requirement of time-reversal and spatial symmetry in previous Z_2 topology theory, resulting in a Z classification with the conventional Z index in a new vector-formed expression called "chiral phase index" (CPI). Our approach is applicable to GNRs of arbitrary terminations and any quasi one-dimensional chiral structures, including magnetism. It naturally solves a recent experimental puzzle of junction states at a class of asymmetric GNR junctions. We moreover derive a simple analytic formula for the CPI of armchair GNRs. Since this approach enables access to electron spin behavior, based on the CPI, we design a novel GNR with periodic localized moments and strong spin−spin exchange coupling.

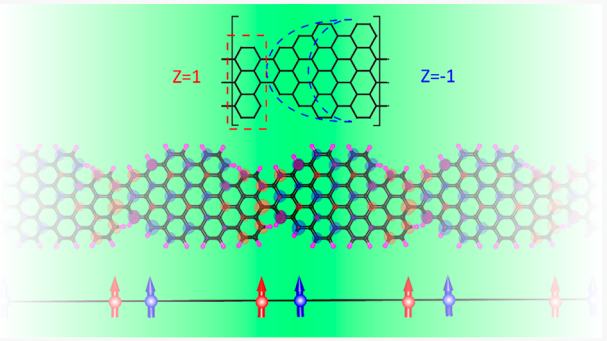

KEYWORDS: *graphene nanoribbons, topology, chiral symmetry, spin chain, strong spin correlations*

Topology classification theory has broadly been applied to explain many physical phenomena such as quantum Hall insulators,[1−5] quantum spin Hall insulators,[6,7] topological insulators, and superconductors.[8−12] However, the power of topology theory has not been as widely used in quasi one-dimensional (1D) systems. The recently developed bottom-up molecular precursors technique enables the synthesis of atomically precise graphene nanoribbons (GNRs).[13−16] These structurally precise 1D materials, with different structures, have been predicted to possess band gaps due to quantum confinement and interaction effects,[17,18] while graphene is a semimetal. Since the discovery of distinct topological phases in GNRs,[19] topology classification in GNRs has proven to be highly successful in predicting the emergence of topological in-gap states localized at the boundaries and junctions of such GNRs.[19−22] However, for example, the topological origin of the observed robust junction states between a bearded termination of armchair GNRs[23] (AGNRs) and of the formation of a metallic 5-sawtooth-GNRs (5-sGNRs) based on in-gap states[24] between segments of AGNRs is still unclear. In the former kind of junctions [Figure 1c], as spatial symmetry in the commensurate unit cell on both sides of the junction does not exist, the previous Z_2 topology theory based on spatial symmetry[19] loses its predictive power. To overcome this conceptual issue, we utilize the topology classification theory using chiral symmetry[11,12,25,26] and apply this approach to GNRs. Chiral symmetry generally exists in a honeycomb structure of similar atoms if the second-nearest-neighbor interaction can be neglected. As discussed below, we note that spatial and time-reversal symmetries can exist exactly in many 1D structures (even with a strong second-nearest-neighbor interaction); however, chiral symmetry can be used as an excellent approximate symmetry for GNR structures, especially when other symmetries do not exist.

Mathematically, chiral symmetry for a system with Hamiltonian H refers to having an operation Γ satisfying[11]

$$H = -\Gamma H \Gamma^{-1},\ \Gamma\Gamma^{\dagger} = 1,\ \Gamma^2 = 1 \tag{1}$$

The operation Γ does not depend on any specific spatial coordinates, and thus it can easily be preserved when a crystal system is terminated at a boundary. Chiral symmetry exists in bipartite lattices, in which the system can be divided into two sublattices, A and B, such that after an appropriate energy shift there are only *nonzero* interaction matrix elements between basis functions on the different sublattices. For such a system, eq 1 is satisfied by using an atomic-site orbital basis and setting Γ to a diagonal matrix with matrix elements equal to 1 for the A sublattice part and −1 for the B sublattice part. Graphene is a bipartite lattice system within a tight-binding formalism, with *only* first-nearest-neighbor hopping included. Within this spirit, we may analyze the electron topological properties of GNRs orany other approximate bipartite 1D structures, using chiral

Received: September 1, 2020
Revised: December 7, 2020
Published: December 15, 2020

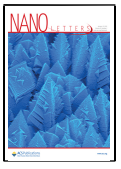

https://dx.doi.org/10.1021/acs.nanolett.0c03503
Nano Lett. 2021, 21, 197−202

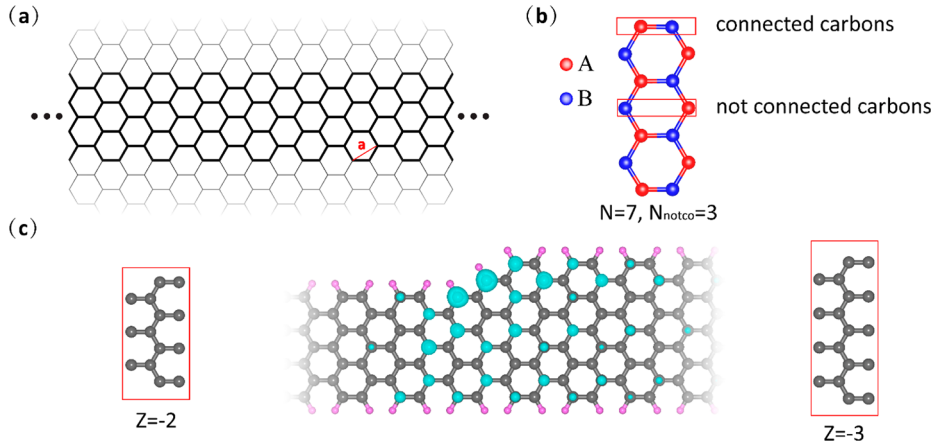

Figure 1. AGNR is specified by the number of carbon rows N forming its width, labeled as N-AGNR. (a) Structure of 7-AGNR (bold region) from the graphene backbone background. a is the length of the lattice vector of graphene. The σ-bond of the edge atoms of GNRs are typically passivated by hydrogen atoms in experiment. (b) Unit cell of a 7-AGNR with zigzag termination, the rows with two carbon connected by a σ-bond within the unit cell (connected carbons), and the rows with two carbon not connected by a σ-bond within the unit cell (not connected carbons) are indicated. This case corresponds to having three rows of not-connecting pairs, $N_{\mathrm{notco}} = 3$. (c) An asymmetric junction of 7-AGNR and 9-AGNR with bearded termination. The corresponding commensurate bulk unit cells for the two segments are shown on the sides, and the 5% isosurface of the wave function square (blue color) of the in-gap junction state from DFT-LDA calculation is shown in the middle.

symmetry, and treat subsequently small second-nearest-neighbor or other chiral-symmetry-breaking effects perturbatively.

To derive the bulk index for the GNRs and other bipartite quasi-1D systems, we use a first-nearest-neighbor tight-binding model and follow the standard Fermion-projector method.[11,12] The Fermion projector is a Hermitian operator defined as

$$Q_k = \sum_{n}^{N_{unocc}} |\psi_{nk}\rangle\langle\psi_{nk}| - \sum_{m}^{N_{occ}} |\psi_{mk}\rangle\langle\psi_{mk}| \tag{2}$$

where $|\psi_{\mathrm{nk}}\rangle$ stands for Bloch states of band n and wavevector k. N_{unocc} is the number of unoccupied bands, and $N_{\mathrm{occ}} = N_{\mathrm{unocc}}$ is the number of occupied bands. Q_{k} can be understood as a continuous deformation of the original Hamiltonian in k-space H_{k}, which has a gapped spectrum around the charge-neutrality energy, by moving energies of the occupied bands to -1 and unoccupied ones to $+1$, while keeping the eigenvectors unchanged. Under chiral symmetry, Q_{k} could be brought into an off-diagonal form using localized site basis (see eq 5 below).

$$Q_{\mathrm{k}} = \begin{bmatrix} 0 & U_{\mathrm{k}} \\ U_{\mathrm{k}}^{\dagger} & 0 \end{bmatrix} \tag{3}$$

Combined with the above properties, it was proved that U_{k} belongs to a unitary group $U(N_{\mathrm{occ}})$; the classification is given by the homotopy group $\pi_1(U(N_{\mathrm{occ}})) = Z$, and the bulk index is the first odd Chern number written as[25,26]

$$\mathrm{Ch}_1(U) = \frac{-i}{2\pi}\int_{1\mathrm{DBZ}} Tr(U_{\mathrm{k}}^{\dagger}\partial_{\mathrm{k}}U_{\mathrm{k}})\ \mathrm{d}k \tag{4}$$

Although eq 4 has been broadly used in mathematics, it is inconvenient to use the matrix form to evaluate physical quantities. Here, we use the properties of the wave functions under chiral symmetry to bring the bulk index given in eq 4 equivalently into a vector form, which we shall call such bulk index for reasons below as a chiral phase index (CPI).

From eq 1, a Hamiltonian with chiral symmetry anticommutes with the chiral operator Γ of a bipartite lattice. This brings the following properties to the wave functions.

$$\Gamma\begin{pmatrix}\alpha_{\mathrm{nk}}\\ \beta_{\mathrm{nk}}\end{pmatrix}_E = \begin{pmatrix}\alpha_{\mathrm{mk}}\\ \beta_{\mathrm{mk}}\end{pmatrix}_{-E} = \begin{pmatrix}\alpha_{\mathrm{nk}}\\ -\beta_{\mathrm{nk}}\end{pmatrix}_E \tag{5}$$

The subscripts E and $-E$ represent the eigenvalues of the Hamiltonian H. α_{nk} and β_{nk} are vectors representing the A sublattice components and the B sublattice components, respectively. Combining eqs 2−5 and using the orthogonalization properties of wave functions (see the Supporting Information), we derive from eq 4 the CPI.

$$Z = \frac{-i}{\pi}\sum_{n\in\mathrm{occ}} \mathrm{inter}\left(\int_{1\mathrm{DBZ}} \langle u_{\mathrm{nk}}|\Gamma\partial_{\mathrm{k}}|u_{\mathrm{nk}}\rangle\ \mathrm{d}k\right) \tag{6}$$

Here *inter* means taking only the intercell part of the above expression.[27] u_{nk} is the periodic part of the Bloch states. Using eq 5, we may write the Z index as

$$Z = \frac{-i}{\pi}\int_{1\mathrm{DBZ}} \mathrm{d}k \sum_{n\in\mathrm{occ}} (\alpha_{\mathrm{nk}}^{\dagger}\partial_{\mathrm{k}}\alpha_{\mathrm{nk}} - \beta_{\mathrm{nk}}^{\dagger}\partial_{\mathrm{k}}\beta_{\mathrm{nk}}) \tag{7}$$

Eq 7 requires only the knowledge of the occupied wave functions, rather than full information on the Hamiltonian matrix, and it is very convenient in calculating the bulk-index analytically. We want to point out that the CPI is very different from that of an index obtained with the intercell part of the Zak phase used in the previous work;[19,28,29] namely, the intercell Zak phase is given by $\sum_{n\in\mathrm{occ}} \mathrm{inter}\left(\int_{1\mathrm{DBZ}} \langle u_{\mathrm{nk}}|\partial_{\mathrm{k}}|u_{\mathrm{nk}}\rangle\ \mathrm{d}k\right)$. The CPI is determined by the *difference* between the intercell part of the Zak phase contributed by the A sublattice and that contributed by the B sublattice rather than the sum of these two parts, and it yields a Z classification rather than a Z_2 classification.

An important general consequence of eq 6 is that the CPI is fully gauge-invariant (see the Supporting Information) and only defined for the charge neutrality gap, since chiral symmetry in the form of eq 3 has been used.

https://dx.doi.org/10.1021/acs.nanolett.0c03503
Nano Lett. 2021, 21, 197−202

As a gauge-invariant quantity, the CPI is expected to be a measurable quantity. While the Zak phase in 1D connects with the modern theory of polarization,[30] the CPI can be related to the difference between the electric dipole moments per unit cell of the two sublattices. However, a most straightforward way of measuring CPI would be by counting the number of topological end states at the end of the system with vacuum. This quantity is connected to the bulk index (of a unit cell commensurate to the boundary termination) by using the bulk-boundary correspondence given in ref 26 as $Z_{\text{bulk}} = N_+ - N_-$ for a system that is terminated to the right. $N_{+(-)}$ is the number of zero mode with positive (negative) chirality. States with positive (negative) chirality localize only on the A (B) sublattice. (For an AGNR, the convention used here is that, for any carbon pairs connected by horizontal $\sigma\sigma$-bond, the atom on the left is denoted as sublattice A, and that on the right is denoted as sublattice B. See Figure 1b.) The number of protected in-gap end states would be equal to the number of midgap states of one chirality in excess over the other chirality, since pairs of states of opposite chirality can interact through perturbations at the end and move out of the bulk gap. In short, through the bulk-boundary correspondence, the CPI contains two pieces of important information at the termination of the system. First, $|Z|$ gives the number of end states that are protected by a chiral symmetry, and second, $\text{sgn}(Z)$ gives the chirality of the end states.[26] Moreover, the bulk-boundary correspondence applies when two such bulk materials with distinct CPIs are joined and topological-protected junction states are formed. One can show that the number of topological junction states, as two bulk structures with bulk index $Z^{\text{left}}_{\text{bulk}}$ and $Z^{\text{right}}_{\text{bulk}}$ are joined, is $N_+ - N_- = Z^{\text{left}}_{\text{bulk}} - Z^{\text{right}}_{\text{bulk}}$. The nature of topology classification ensures that these junction states are immune to any perturbations preserving chiral symmetry, and they remain qualitatively unchanged under perturbations violating chiral symmetry that are relatively small in strength compared to the band gap.

We now obtain an explicit expression for the CPI of AGNRs with different widths and end terminations using eq 7. The tight-binding wave functions of the GNRs may be analytically calculated from a linear combination of graphene's wave functions with proper boundary conditions[19] (see the Supporting Information). After the resulting wave functions are inserted into eq 7, a general formula of the Z index for an arbitrary AGNR with any commensurate unit cell is derived as (see the Supporting Information)

$$Z = N_{\text{notco}} - \left\lfloor \frac{N}{3} \right\rfloor \tag{8}$$

Here N is the total number of rows of carbon atoms forming the width of the AGNR,[17] and N_{notco} is the number of rows of atoms with carbon pairs not connected by σ-bonds within the specific unit cell that is commensurate to an anticipated termination. The topless brackets denote the floor function, which takes the largest integer less than or equal to the value within the brackets. The definition of connected carbon pairs (with distance close to $a/\sqrt{3}$) and unconnected pairs (with distance close to $\sqrt{3}a/2$) is shown in Figure 1b. Eq 8 is deceptively compact and simple, as well as easy to evaluate, yet an essential finding of the analysis.

With the Z classification using chiral symmetry, the in-gap junction states localized at the asymmetric junction in Figure 1 formed by bearded termination of 7-AGNR and 9-AGNR observed in experiment[23,24] could now be well-explained. The bearded 7-AGNR unit cell has $Z = -2$, while the bearded 9-AGNR unit cell has $Z = -3$, giving rise to one protected in-gap state at the junction as confirmed by our explicit density functional theory (DFT) calculations within the local-density approximation (LDA) as implemented in the Quantum Espresso package.[31] Since $Z^{\text{left}}_{\text{bulk}} - Z^{\text{right}}_{\text{bulk}} = +1$, the junction state has amplitudes only on the A sublattice (Figure 1c).

Equation 8 can be applied to AGNRs of any general termination types that preserve chiral symmetry, not limited to the common studied zigzag, zigzag′, or bearded types.[19] As shown in Figure 2a, the zigzag termination of 7-AGNR has $Z =$ 1, and the "bullet" termination of 9-AGNR has $Z = -1$. When terminated to the vacuum, one in-gap end state exists at the termination of each structure. Nevertheless, the two corresponding bulk structures belong to different classes because of the opposite signs of the CPI. Two topologically protected junction states should occur when these two structures are joined, as confirmed by a DFT-LSDA calculation (Figure 2b). A simple physical understanding of why these two in-gap localized states do not hybridize significantly with each other at the junction and move out of the gap is that they are localized on the same sublattice. Any interaction allowing hopping between the same sublattice would have to break chiral symmetry. In principle, for physical AGNR junctions, there may be a small energy splitting between the two junction states due to second-nearest-neighbor hopping. Our DFT-LSDA results show that such a splitting due to the breaking of chiral symmetry is minimal in this case.

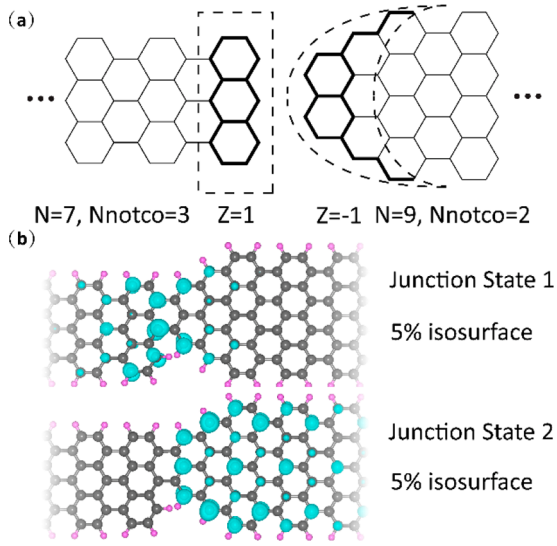

Figure 2. (a, left) A 7-AGNR with zigzag termination is shown; the unit cell commensurate with the termination has three rows of unconnected carbons pairs, and Z = 1. (a, right) A bullet termination of 9-AGNR is shown. Its commensurate unit cell has two rows of unconnected carbons pairs, and $Z = -1$. (b) Joining the two structures in (a) results in a junction with $\Delta Z = 2$, giving rise to two in-gap junction states. The 5% isosurface of the wave function square of the two junction states from a DFT-LSDA (LSDA = local-spin-density approximation) calculation is shown in blue. Here only the occupied spin-up states are shown. One state localizes in the 7-AGNR region; the other localizes in the 9AGNR region.

Remarkably, if the electron spin degree of freedom is considered, the junction states depicted in Figure 2b would couple to each other ferromagnetically if one can arrange for

https://dx.doi.org/10.1021/acs.nanolett.0c03503
Nano Lett. 2021, 21, 197−202

the atomic structure of such a junction to have locally a sublattice imbalance of two carbon atoms, according to Lieb's theorem.[32] And if such junctions were repeated into a 1D superlattice, a 1D ferromagnetic spin chain would form. The inset in Figure 3a illustrates the unit cell of such a superlattice

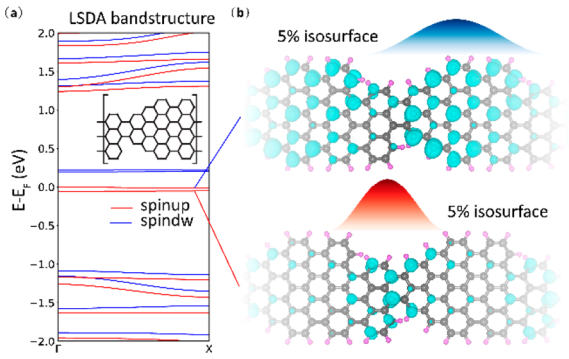

Figure 3. (a) Computed DFT-LSDA band structure of a periodic GNR spin chain structure (unit cell shown by insert). Top of the occupied bands is set at zero. The in-gap bands (in window −0.1−0.3 eV) are nearly flat, indicating negligible hopping between neighboring junction states. A spin splitting of 0.2 eV occurs between oppositely oriented spin bands; the two majority-spin (spin-up) bands are occupied, leaving their spin-down counterparts empty. Each unit cell has 2 bohr magnetons of magnetization. (b) The isosurface at 5% of the wave function square of the two occupied junction states at $k = \Gamma$ is shown (blue color). One is localized in the 9-AGNR region, while the other is localized in the 7-AGNR region.

we designed. Since each superlattice unit cell has a sublattice imbalance of two atoms, we have a net magnetization of 2 bohr magnetons per unit cell. As normally the onsite Coulomb U is small in strength compared to the hopping term t in a π-orbital system, we use a mean-field calculation to manifest the effect of a Hubbard model considered in Lieb's theorem. Here we perform a DFT-LSDA calculation and find that the magnetization is mainly contributed by the two occupied symmetry-protected junction states (Figure 3), in agreement with the conclusion of our topology theory and Lieb's theorem. Since the direct exchange coupling J between two electron spins is proportional to their wave function overlap, having the two states mainly localized near the same junction is expected to give rise to a strong exchange coupling. To analyze the magnetic properties of such a chain, we map the LSDA results to those of a 1D Ising model Hamiltonian with two spins per unit cell.

$$H = \sum_i J_1 \hat{s}_{i1z}\hat{s}_{i2z} + J_2 \hat{s}_{i2z}\hat{s}_{i+1,1z} \tag{9}$$

where i denotes the unit cell index. To extract the coupling strengths J_1 and J_2 from first-principles calculations, we consider three different spin configurations shown in Figure 4b and perform DFT-LSDA studies. The three configurations correspond to states with total energy per unit cell of $\frac{1}{4}J_1 + \frac{1}{4}J_2$, $-\frac{1}{4}J_1 - \frac{1}{4}J_2$, and $\frac{1}{4}J_1 - \frac{1}{4}J_2$, respectively. Using the total energy differences from our first-principles calculations under constrained LSDA, we obtain $J_1 = -87$ meV/$\hbar^2$ and $J_2 = -30$ meV/$\hbar^2$, making them parameters for a stronger ferromagnetic (FM) 1D system compared to what has been achieved before.[33] Since exchange coupling decays exponentially with distance,[19] we estimate the second-nearest neighbor exchange to be around −6 meV/$\hbar^2$ and can be ignored in our model.

Because of thermal fluctuation effects, it is known that there is no long-range magnetic order at finite temperature in 1D structures with isotropic spin interactions, according to the Mermin-Wagner theorem.[34] Thus, the meaningful quantity one should consider is the spin−spin correlation length. As a rough estimate of this quantity, we may use a canonical ensemble of 1D Ising model with partition function.

$$Z = \sum_{\{s_{ai}\}} e^{-\beta H(\{s_{ai}\})} \tag{10}$$

The spin−spin correlation length, defined as $a = -R/\ln\langle s_{\alpha i} s_{\alpha,\, i+R}\rangle$, where R is the distance between two spins and can be calculated analytically by treating the spins classically. Evaluating the expectation value and expressing it as a function of the coupling strengths and temperature, we have[35]

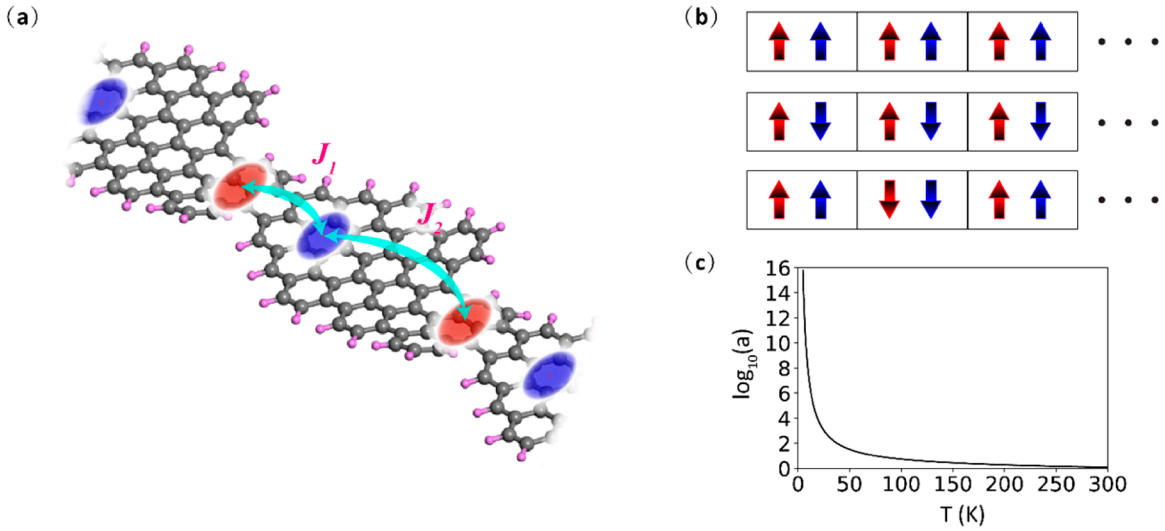

Figure 4. (a) Schematic of a 1D GNR spin chain (Figure 3) and exchange interactions (J_1 and J_2). (b) Three different spin configurations are considered in first-principles DFT-LSDA calculations to extract the exchange coupling parameters. (c) Spin−spin correlation length (in unit of lattice vector and log scale) as a function of temperature from a classical canonical ensemble of 1D Ising model.

https://dx.doi.org/10.1021/acs.nanolett.0c03503
Nano Lett. 2021, 21, 197−202

$$a = -\frac{2}{\ln(|\tanh \beta J_1|) + \ln(|\tanh \beta J_2|)} \quad (11)$$

where $\beta = 1/k_B T$. The temperature dependence of the correlation length in this model is plotted in Figure 4c. At 3 K (at which low temperature Scanning Tunneling Microscope (STM) measurements typically are done), the spin correlation length is expected to be at the tens-of-nanometers scale. Although constraining the spin direction in an Ising model would overestimate the spin−spin correlation length, the spin−spin correlation length would still be over tens of nanometers, considering a classical Heisenberg model.[36] The strong coupling strength and long correlation length of such designed GNRs should open up applications to spin qubits[37] and spin-dependent transport[38] through nanostructures.

As a final remark, we point out that the present classification theory, together with our simple analytic expression for Z of AGNRs, could be applied generally to generate a variety of spin configurations. One could design junctions with arbitrary numbers of coupled localized spin states, and, by controlling how the junctions are connected, either FM or anti-FM coupling between junctions could be realized. The theory may also be applied to other 1D chiral structures, such as the 1D chiral GNRs, which could be synthesized.[39]

METHOD

First-principles DFT calculations in the local-density approximation and local spin-density approximation are done using the Quantum Espresso packages.[31] A supercell geometry is used with a 15 Å vacuum spacing applied to each of the nonperiodic directions of the nanoribbons to avoid interaction between replicas. The atomic geometry of the junction and spin chain structure is fully relaxed, until all components of the forces on each atom are smaller than 0.01 eV/Å. Scalar relativistic and norm-conserving pseudopotentials of C and H are used.[31]

After this paper was written and submitted to the arXiv, we became aware of another work on the arXiv[40] that also uses chiral symmetry to classify 1D bipartite models.

ASSOCIATED CONTENT

Supporting Information

The Supporting Information is available free of charge at https://pubs.acs.org/doi/10.1021/acs.nanolett.0c03503.

> Topology classification using chiral symmetry and spin correlations in graphene nanoribbons. Deriving the chiral phase index. Proving gauge-invariant of CPI. General bulk-index formula for the case of AGNRs. Isosurface of spin-down states of a periodic spin-chain. Stability of the electronic structure upon charge doping for a sawtooth AGNR spin-chain structure (PDF)

AUTHOR INFORMATION

Corresponding Author

Steven G. Louie − *Department of Physics, University of California, Berkeley, California 94720, United States; Materials Sciences Division, Lawrence Berkeley National Laboratory, Berkeley, California 94720, United States;* orcid.org/0000-0003-0622-0170; Phone: +1-510-642-1709; Email: sglouie@berkeley.edu

Author

Jingwei Jiang − *Department of Physics, University of California, Berkeley, California 94720, United States; Materials Sciences Division, Lawrence Berkeley National Laboratory, Berkeley, California 94720, United States;* orcid.org/0000-0002-0949-4401

Complete contact information is available at: https://pubs.acs.org/10.1021/acs.nanolett.0c03503

Author Contributions

S.G.L. conceived and directed the research, and J.J. developed the analytic chiral topological index for GNRs and carried out the calculations.

Notes

The authors declare no competing financial interest.

ACKNOWLEDGMENTS

We acknowledge helpful discussions with F. Zhao, Z. L. Li, M. Wu, and T. Cao. This work is supported by Office of Naval Research MURI under Award No. N00014-16-1-2921 (topology theory) and by the National Science Foundation DMR-1926004 (LSDA simulations and spin physics analysis). Computational resources were provided by the Department of Energy at Lawrence Berkeley National Laboratory's NERSC facility, the National Science Foundation through XSEDE resources at NICS, and through Frontera computing project at the Texas Advanced Computing Center under Award No. OAC-1818253.

ABBREVIATIONS

GNRs, graphene nanoribbons
CPI, chiral phase index
1D, one-dimensional
AGNRs, armchair graphene nanoribbons
5-sGNRs, 5-sawtooth GNRs
DFT, density functional theory
LDA, local-density approximation
LSDA, local-spin-density approximation
FM, ferromagnetic

REFERENCES

(1) Klitzing, K. V.; Dorda, G.; Pepper, M. New Method for High-Accuracy Determination of the Fine-Structure Constant Based on Quantized Hall Resistance. *Phys. Rev. Lett.* **1980**, *45*, 494.
(2) Laughlin, R. B. Quantized Hall Conductivity in Two Dimensions. *Phys. Rev. B* **1981**, *23*, 5632R.
(3) Thouless, D. J.; Kohmoto, M.; Nightingale, M. P.; denNijs, M. Quantized Hall Conductance in a Two-Dimensional Periodic Potential. *Phys. Rev. Lett.* **1982**, *49*, 405.
(4) Halperin, B. I. Quantized Hall Conductance, Current-carrying Edge States, and the Existence of Extended States in a Two-dimensional Disordered Potential. *Phys. Rev. B: Condens. Matter Mater. Phys.* **1982**, *25*, 2185.
(5) Hatsugai, Y. Chern Number and Edge States in the Integer Quantum Hall Effect. *Phys. Rev. Lett.* **1993**, *71*, 3697.
(6) Bernevig, B. A.; Hughes, T. L.; Zhang, S.-C. Quantum Spin Hall Effect and Topological Phase Transition in HgTe Quantum Wells. *Science* **2006**, *314*, 1757.
(7) König, M.; et al. Quantum Spin Hall Insulator State in HgTe Quantum Wells. *Science* **2007**, *318*, 766.
(8) Qi, X.-L.; Zhang, S.-C. Topological Insulators and Superconductors. *Rev. Mod. Phys.* **2011**, *83*, 1057.
(9) Kitaev, A.; et al. Periodic Table for Topological Insulators and Superconductors. *AIP Conf. Proc.* **2008**, *1134*, 22.

(10) Zirnbauer, M. R. Riemannian Symmetric Superspaces and their Origin in Random-matrix Theory. *J. Math. Phys.* **1996**, *37*, 4986.
(11) Schnyder, A. P.; Ryu, S.; Furusaki, A.; Ludwig, A. W. W. Classification of Topological Insulators and Superconductors in Three Spatial Dimensions. *Phys. Rev. B: Condens. Matter Mater. Phys.* **2008**, *78*, 195125.
(12) Schnyder, A. P.; Ryu, S.; Furusaki, A.; Ludwig, A. W. W.; et al. Classification of Topological Insulators and Superconductors. *AIP Conf. Proc.* **2008**, *1134*, 10.
(13) Chen, Y.-C.; et al. Tuning the Band Gap of Graphene Nanoribbons Synthesized from Molecular Precursors. *ACS Nano* **2013**, *7*, 6123−6128.
(14) Cai, J.; et al. Atomically Precise Bottom-up Fabrication of Graphene Nanoribbons. *Nature* **2010**, *466*, 470.
(15) Ruffieux, P.; et al. On-surface Synthesis of Graphene Nanoribbons with Zigzag Edge Topology. *Nature* **2016**, *531*, 489.
(16) Talirz, L.; et al. On-Surface Synthesis and Characterization of 9-Atom Wide Armchair Graphene Nanoribbons. *ACS Nano* **2017**, *11*, 1380−1388.
(17) Son, Y.-W.; Cohen, M. L.; Louie, S. G. Energy Gaps in Graphene Nanoribbons. *Phys. Rev. Lett.* **2006**, *97*, 216803.
(18) Yang, L.; Park, C.-H.; Son, Y.-W.; Cohen, M. L.; Louie, S. G. Quasiparticle Energies and Band Gaps in Graphene Nanoribbons. *Phys. Rev. Lett.* **2007**, *99*, 186801.
(19) Cao, T.; Zhao, F.; Louie, S. G. Topological Phases in Graphene Nanoribbons: Junction States, Spin Centers, and Quantum Spin Chains. *Phys. Rev. Lett.* **2017**, *119*, No. 076401.
(20) Zhao, F.; Cao, T.; Louie, S. G. Electric Field Tunable Topological Phases in Graphene Nanoribbons. Manuscript in preparation.
(21) Lee, Y.-L.; Zhao, F.; Cao, T.; Ihm, J.; Louie, S. G. Topological Phases in Cove-Edged and Chevron Graphene Nanoribbons: Geometric Structures, 2 Invariants, and Junction States. *Nano Lett.* **2018**, *18* (11), 7247−7253.
(22) Rizzo, D. J.; et al. Topological Band Engineering of Graphene Nanoribbons. *Nature* **2018**, *560*, 204−208.
(23) Gröning, O.; et al. Engineering of Robust Topological Quantum Phases in Graphene Nanoribbons. *Nature* **2018**, *560*, 209−213.
(24) Rizzo, D. J.; et al. Inducing Metallicity in Graphene Nanoribbons via Zero-Mode Superlattices. *Science* **2020**, *369*, 1597−1603.
(25) Ryu, S.; et al. Topological Insulators and Superconductors: Tenfold Way and Dimensional Hierarchy. *New J. Phys.* **2010**, *12*, No. 065010.
(26) Prodan, E.; Schulz-Baldes, H. *Bulk and Boundary Invariants for Complex Topological Insulators;* Springer International Publishing: Basel, Switzerland, 2016.
(27) Rhim, J.-W.; Behrends, J.; Bardarson, J. H. Bulk-boundary Correspondence from the Intercellular Zak phase. *Phys. Rev. B: Condens. Matter Mater. Phys.* **2017**, *95*, No. 035421.
(28) Lin, K.-S.; Chou, M.-Y. Topological Properties of Gapped Graphene Nanoribbons with Spatial Symmetries. *Nano Lett.* **2018**, *18*, 7254−7260.
(29) Delplace, P.; Ullmo, D.; Montambaux, G. Zak Phase and the Existence of Edge States in Graphene. *Phys. Rev. B: Condens. Matter Mater. Phys.* **2011**, *84*, 195452.
(30) Resta, R. Macroscopic Polarization in Crystalline Dielectrics: the Geometric Phase Approach. *Rev. Mod. Phys.* **1994**, *66*, 899.
(31) Giannozzi, P.; et al. QUANTUM ESPRESSO: a Modular and Open-source Software Project for Quantum Simulations of Materials. *J. Phys.: Condens. Matter* **2009**, *21*, 395502.
(32) Lieb, E. H. Two Theorems on the Hubbard Model. *Phys. Rev. Lett.* **1989**, *62*, 1927.
(33) Slota, M.; et al. Magnetic Edge States and Coherent Manipulation of Graphene Nanoribbons. *Nature* **2018**, *557*, 691−695.
(34) Mermin, N. D.; Wagner, H. Absence of Ferromagnetism or Antiferromagnetism in One- or Two-Dimensional Isotropic Heisenberg Models. *Phys. Rev. Lett.* **1966**, *17*, 1133.
(35) Lévy, L. P. *Magnetism and Superconductivity;* Springer: Berlin, Germany, 2000,.
(36) Yazyev, O. V.; Katsnelson, M. I. Magnetic Correlations at Graphene Edges: Basis for Novel Spintronics Devices. *Phys. Rev. Lett.* **2008**, *100*, No. 047209.
(37) Trauzettel, B.; Bulaev, D. V.; Loss, D.; Burkard, G. Spin Qubits in Graphene Quantum Dots. *Nat. Phys.* **2007**, *3*, 192−196.
(38) Nguyen, V. H.; et al. Spin-dependent Transport in Armchair Graphene Nanoribbon Structures with Edge Roughness Effects. *J. Phys.: Conf. Ser.* **2009**, *193*, No. 012100.
(39) de Oteyza, D. G.; et al. Substrate-Independent Growth of Atomically Precise Chiral Graphene Nanoribbons. *ACS Nano* **2016**, *10* (9), 9000−9008.
(40) Guzmán, M.; Bartolo, D.; Carpentier, D. Geometry and Topology Tango in Chiral Materials*arxiv*[cond-mat.str-el], February 7, 2020, 2002.02850, ver. 1, https://arxiv.org/abs/2002.02850 (accessed 2020-11-23).

https://dx.doi.org/10.1021/acs.nanolett.0c03503
Nano Lett. 2021, 21, 197−202